Clinical Response to Neurofeedback in Major Depression Relates to Subtypes of Whole-Brain Activation Patterns During Training

Masaya Misaki Ph.D.[a,b*], Kymberly D. Young Ph.D.[c], Aki Tsuchiyagaito Ph.D.[a,b], Jonathan Savitz Ph.D.[a,b], and Salvador M. Guinjoan M.D. Ph.D.[a,b,d]

[a] Laureate Institute for Brain Research, Tulsa, OK, USA
[b] Oxley College of Health and Natural Sciences, The University of Tulsa, Tulsa, OK, USA
[c] Department of Psychiatry, University of Pittsburgh School of Medicine, Pittsburgh, PA, USA
[d] Department of Psychiatry, Oklahoma University Health Sciences Center at Tulsa, Tulsa, OK, USA

*Corresponding author:
Masaya Misaki
Laureate Institute for Brain Research
6655 South Yale Avenue
Tulsa, OK 74136 USA
mmisaki@laureateinstitute.org
TEL: +1-918-502-5137
FAX: +1-918-502-5135

Abstract

Major Depressive Disorder (MDD) presents a significant public health challenge. Real-time functional magnetic resonance imaging neurofeedback (rtfMRI-NF) shows promise as a treatment for this disorder, although its mechanisms of action remain unclear. This study investigated whole-brain response patterns during rtfMRI-NF training to explain interindividual variability in clinical efficacy in MDD. We analyzed data from 95 participants (67 active, 28 control) with MDD from previous rtfMRI-NF studies designed to increase left amygdala activation through positive autobiographical memory recall. We focused on whole-brain activation patterns during two critical epochs of the neurofeedback procedure: activation during the self-regulation period and transient responses to feedback signal presentation. Through a systematic process involving feature selection, manifold extraction, and clustering with cross-validation, we identified subtypes within these patterns. Significant symptom reduction was observed in the active group (t=-4.404, d=-0.704, p<0.001) but not in the control group (t=-1.609, d=-0.430, p=0.111); however, left amygdala activation did not account for the variability in clinical efficacy. Subtyping analysis revealed two subtypes in regulation activation and three subtypes in brain responses to feedback signals (regulation: F=8.735, p=0.005; feedback response: F=5.326, p=0.008; interaction: F=3.471, p=0.039). Subtypes associated with significant symptom reduction were characterized by selective increases in control regions, including lateral prefrontal areas, and decreases in regions associated with self-referential thinking, such as default mode areas. These findings suggest that large-scale brain activity is more critical for clinical efficacy than the level of activation in the neurofeedback target region during training. Tailoring neurofeedback training to incorporate these patterns could significantly enhance its therapeutic efficacy.

Introduction

Major Depressive Disorder (MDD) presents a significant public health challenge, with approximately one-third of diagnosed patients not responding to first-line treatments such as antidepressants and psychotherapy. This results in substantial disability and economic losses due to treatment costs and lost productivity [1, 2]. Real-time functional magnetic resonance imaging neurofeedback (rtfMRI-NF) has emerged as a promising alternative, demonstrating large to medium effect sizes in treating depressive symptoms [3-5] without significant reported adverse effects [6]. This noninvasive brain modulation technique involves the real-time analysis and visualization of brain activation signals, thereby enabling participants to self-regulate their brain activity. Its efficacy in training participants to modulate their brain activation is well-supported by numerous studies, including several meta-analyses [3-11]. However, the direct impact of rtfMRI-NF on symptom relief is not yet fully understood due to incomplete knowledge of the neural mechanisms by which this training alleviates symptoms through the regulation of specific brain activations.

Previous studies on the mechanisms of NF training have identified a broad spectrum of brain activities associated with NF-mediated self-regulation training [12-15], including investigations into brain responses to feedback signals [15-19]. Two types of brain activation, evaluation of feedback values and modulation of brain activation, are common components of the reinforcement learning process [20] and are crucial for elucidating the learning mechanisms of NF-mediated brain regulation. Active regions during these epochs typically include the prefrontal cortex, salience network, and reward processing areas [12-15]. However, while many studies have focused on the success of regulating target brain activities, the relationship between these activities and subsequent symptom relief remains elusive. Furthermore, interindividual variability in the clinical efficacy of NF necessitates further investigation to identify brain response subtypes associated with therapeutic outcomes.

This study aimed to characterize whole-brain activation patterns during rtfMRI-NF training in individuals with MDD, with the goal of identifying brain activation subtypes associated with interindividual variability in therapeutic efficacy. To this end, we analyzed a large dataset from rtfMRI-NF studies where participants with MDD were trained to regulate left amygdala activity through neurofeedback [21-24]. These studies consistently observed significant reductions in depressive symptoms on average post-training, albeit with variations in therapeutic outcomes among participants.

We hypothesized that the observed variability in treatment efficacy could be explained by variations in whole-brain activation patterns during self-regulation training, extending beyond the NF target region (amygdala). The involvement of large-scale networks in NF training has been demonstrated in a meta-analysis of NF studies [12], and evidence suggests that the effects of NF training may extend beyond the targeted brain region [25-27]. Specifically, we focused on two types of brain activation critical for NF training: regulatory task activity throughout the task block and instantaneous responses to neurofeedback signal presentation (Figure 1). These two types of activation are thought to correspond to two critical components of the reinforcement learning process [20] and may characterize the training process for each individual.

Methods

Participants

The present study was a secondary analysis of data from our previously published studies [21, 22, 24] and a preliminary study utilizing the same rtfMRI-NF protocols in individuals diagnosed with MDD. The University of Oklahoma Institutional Review Board (IRB) or the Western IRB reviewed and approved the study protocols, ensuring adherence to the ethical principles of the Declaration of Helsinki. Participants provided written informed consent prior to participation and were financially compensated. Participants met DSM-IV-TR [28] criteria for MDD based on the

Structural Clinical Interview for DSM-IV disorders [29] or DSM-5 criteria for MDD based on the Mini-International Neuropsychiatric Interview (MINI) [30]. Previous articles [21, 22, 24] detailed each study's inclusion and exclusion criteria. Common inclusion criteria across studies are ages 18-65, current diagnosis of MDD, and common exclusion criteria are current diagnosis of PTSD, substance use disorder, bipolar disorder, active suicidal ideation or behavior within a year, a history of psychosis, pregnancy, and MRI contraindicators. The present analysis included data from 95 participants with MDD (68 females; mean age ± SD = 33.6 ± 10.4 years), consisting of 67 in the active NF group (46 females) who received left amygdala neurofeedback and 28 in the control group (22 females) who received neurofeedback from a brain region not associated with emotional processing.

Real-time fMRI Neurofeedback Paradigm

The NF training was designed to enhance the activation signal in the left amygdala while recalling happy autobiographical memories [31]. The task sequence utilized a blocked design consisting of alternating periods of rest, self-regulation with NF, and number counting, each lasting 40 seconds. This sequence was repeated four times in a single training run, with participants undergoing three such runs per session. Because the number of sessions differed among the studies, the present analyses were confined to data from the three runs of the initial session. Depressive symptom severity was estimated with the Montgomery-Åsberg Depression Rating Scale (MADRS) [32] immediately before the NF session, and again one-week post-training.

MRI imaging in all experiments was conducted using the same 3T Discovery MR750 scanner (GE Healthcare). Blood Oxygenation Level-Dependent (BOLD) fMRI data acquisition employed a T2*-weighted gradient-echo planar imaging (EPI) sequence, with parameters set as follows: TR/TE = 2000/30 ms, acquisition matrix = 96 × 96, field of view (FOV)/slice thickness = 240 mm/2.9 mm, flip angle = 90°, and 34 axial slices, using a SENSE acceleration factor of 2. EPI images were then reconstructed to a 128x128 matrix, resulting in an fMRI voxel size of

1.875x1.875x2.9 mm³. Anatomical reference was obtained using a T1-weighted magnetization-prepared rapid gradient-echo (MPRAGE) sequence.

A detailed description of the rtfMRI-NF procedure can be found in our previous publications [21, 22, 24]. Briefly, a custom in-house rtfMRI system was utilized for the experiments [31]. For the active group, the NF signal was extracted from the left amygdala, defined by 7-mm diameter spheres centered at Talairach coordinates (x, y, z = -21, -5, -16 mm), and then mapped to each participant's brain space. For the control group, the NF signal was sourced from the horizontal segment of the intraparietal sulcus at Talairach coordinates (-42, -48, 48 mm), a region suggested to be unrelated to emotion regulation [33]. During the happy memory recall block, the NF signal was quantified as the percent signal change from the mean signal in the preceding rest block. The signal was updated every 2 s and visually presented to participants as a red bar.

MRI data processing

The Analysis of Functional NeuroImages (AFNI; http://afni.nimh.nih.gov) software suite was utilized for image processing. After discarding the first three volumes to achieve signal equilibrium, preprocessing steps were conducted: despike and RETROICOR [34] along with respiratory volume per time (RVT) regression [35] were applied for physiological noise correction. This was followed by slice-timing and motion corrections, nonlinear warping to the MNI template brain with resampling to 2 mm³ voxels using the Advanced Normalization Tools (ANTs; http://stnava.github.io/ANTs/), spatial smoothing with a 6 mm full-width at half maximum (FWHM) Gaussian kernel, and scaling of signals to percent change relative to the voxel-wise mean.

Activation during the self-regulation was assessed using a general linear model (GLM) analysis. We extracted the two types of brain response in this process (Fig. 1). The GLM regressors included response models for the regulation and counting blocks, each modeled with a boxcar function convolved with the canonical hemodynamic response function (HRF). The regressor for the regulation block was used for estimating the first type of brain activation,

regulation block activation (Fig. 1). The GLM regressors also included twelve motion parameters (three rotations, three translations, and their temporal derivatives), three principal components of ventricle signals, local white matter signals (ANATICOR) [36], and an event-related regressor for the onset of any condition block (modeled as a delta function convolved with HRF) were included as nuisance covariates. Volumes with frame-wise displacement greater than 0.3 and their preceding volume were censored in the GLM.

Another type of brain response, feedback event-related response (Fig. 1), was evaluated with the additional event-related regressors for each feedback presentation. The response was modeled as a delta function modulated by the feedback amplitude normalized in each run (Fig. 1) and convolved with the HRF. Since the feedback signal was presented during the regulation block and this event regressor could be colinear with the regulation block regressor, we orthogonalized the feedback-response-event regressor with regard to the regulation block regressor. The beta coefficients from the GLM analysis were used as response estimates.

These response estimates were assessed for each block independently using the least squares - separate (LS-S) approach [37], in which separate regressors for the target block and all other blocks were included to estimate the response in a block. This procedure was repeated for each block in separate GLM analyses. The use of this block-wise response facilitates subsequent group analysis using linear mixed-effect model and provides the estimates with better test-retest reliability [38, 39].

Clustering analysis

Clustering analysis was conducted solely on the active group participants to categorize their brain activation patterns. This approach was chosen because including the control group might introduce brain activation patterns with various unspecific effects. Such inclusion could increase the dimensionality of latent subtypes and complicate the extraction of subtypes relevant to the active NF training process.

A significant challenge posed by this analysis is the high dimensionality of the whole-brain beta maps; the problem often referred to as the "curse of dimensionality" [40]. This phenomenon refers to the issues arising in high-dimensional spaces, where distances between points become uniformly large, data points are sparsely distributed, and there is a high risk of overfitting, leading to clustering solutions that are difficult to reproduce.

To address this challenge, we implemented a multi-step strategy to reduce dimensionality and identify an informative space associated with treatment outcomes. Additionally, we employed cross-validation to ensure the clustering solution's stability and reproducibility. Our approach involved (1) aggregating voxel-wise responses into regional averages using a functional brain atlas, (2) removing the regions irrelevant to treatment outcomes, (3) applying Uniform Manifold Approximation and Projection (UMAP) [41] to extract a low-dimensional representation, (4) applying k-means clustering in the UMAP space, and (5) employing repeated cross-validation to assess the robustness of the clustering solution [42]. Figure 2 illustrates the flowchart of the clustering analysis performed to delineate subtypes of brain activation.

Initially, voxel-wise beta values were averaged within each functional region defined by the Shen 268 atlas [43, 44]. This atlas was chosen for its demonstrated performance in various predictive modeling studies [43, 45-49]. The data for each participant are averaged across the three runs or for each run. We tested both approaches as a hyperparameter to test which one yielded the most stable clustering solution. Subsequently, we identified regions correlating with changes in the MADRS score (change relative to the baseline score expressed as a ratio?) after adjusting for the effects of age and sex. A threshold of $p < 0.1$ was used for this selection, prioritizing dimensionality reduction rather than finding significantly related regions. After excluding the regions irrelevant to the treatment outcome, we utilized UMAP for dimensionality reduction, followed by k-means clustering. The UMAP parameters were set to optimize the clustered distribution within the reduced-dimensional space, with ‘n_neighbors’ (the number of neighboring points used in the local manifold approximation) set to 50 and ‘min_dist’ (the

minimum distance apart that points are allowed to be in the low-dimensional representation) set to 0. Subsequently, k-means clustering was executed within the UMAP-defined space.

The stability of the clusters was rigorously evaluated through cross-validation, facilitated by the 'reval' Python package [42]. This involved dividing the dataset into two halves, applying clustering to one half, and then applying the derived clustering rule to the opposite half, and vice versa, to assess the consistency of the cluster labels between the two rules (Fig. 2). This procedure was repeated 10 times, each with a unique data split, to calculate the average stability score. The stability measure is the mean normalized Hamming distance between the two solutions, ranging from 0 to 1. A smaller value indicates a more stable and reproducible solution. Since this measure is larger with a larger number of clusters, it was scaled by the stability of random labeling of the same number of clusters [50].

In summary, these procedures were conducted across the hyperparameter space of response summary (average across runs or a sequence of three runs), UMAP random seed (50 values), UMAP dimension (ranging from 2 to 50), and the number of clusters (ranging from 2 to 5) to find robust clustering with the smallest mean distance between the cross-validated solutions.

Mapping the brain responses in each subtype

After identifying the subtypes, we evaluated the voxel-wise response patterns for each subtype using a linear mixed-effect (LME) model analysis performed voxel-wise with the 'lme4' package [51] in R. This LME analysis was applied to the beta values for each block, run, and participant, incorporating fixed effects for the run, the identified subtype from the clustering analysis, age, and sex, as well as a random effect for participants at the intercept level. The mean response for each subtype was calculated using the 'emmeans' package [52] in R. The mean maps of the subtypes were thresholded at a voxel-wise $p < 0.001$, corrected for cluster size with a $p < 0.05$ using AFNI 3dClustSim.

Statistical testing

LME analysis was performed to investigate changes in MADRS scores one week after a single NF session for both active and control groups. The LME model included fixed effects for time (pre-/post-NF), group (active/control), age, and sex, as well as a random effect for participants at the intercept. We also examined whether treatment efficacy was correlated with NF training performance measures, including the mean NF amplitude, mean left amygdala response during the regulation block, and the change in left amygdala response between the first and the last training runs using linear model analysis.

We then examined whether the identified subtypes of brain activation during NF training were associated with demographic and training performance variables, as well as the depressive symptom score (MADRS) at the baseline and its change post-NF. Each variable was examined using linear model analysis, with subtypes serving as independent variables. The post-hoc analysis for the mean response for each subtype and the difference between the subtypes was performed using the 'emmeans' package, and *p*-values for the post-hoc comparisons were corrected by multivariate *t* adjustment.

In addition, the subtyping rules established in the active group were applied to the control group of participants to assess if similar patterns in MADRS score changes across the subtypes could be observed. The presence of consistent subtype associations with symptom reduction across both active and control groups would suggest the operation of a common treatment mechanism, indicating that NF training efficacy is non-specific to the neurofeedback signal from an emotion-related region.

Results

Data selection

Post-training MADRS scores were not available for two participants. fMRI data from five participants were excluded from analysis due to problems with physiological signal acquisition

(n=2) or excessive head motion (n=2) with more than 30% of time points censored (Framewise Displacement [FD] > 0.3) in all training runs. In addition, four participants exhibited excessive head motion in any one of the training runs were excluded only when analyzing data from a series of three training runs. Analyses were performed using the largest sample size available for each test measure, regardless of missing data on other variables (see Supplementary Information [SI], Section 1). No significant differences in age, sex, and baseline MADRS scores were observed between the active and control groups in any of the selected datasets.

Reduction of depressive symptoms following NF training

Figure 3 illustrates the MADRS scores before and after NF training for each group, with average scores represented by the height of bars and individual participant scores depicted as points connected by lines. LME analysis identified a significant main effect of time. Post-hoc analysis revealed a significant decrease in post-session scores (t = -4.404, d = -0.704, p < 0.001). SI Table S2a provides the ANOVA tables for the LME analysis. While the time-group interaction was not statistically significant, the active group showed a significant symptom reduction (t = -5.576, d = -0.978, p < 0.001) but not the control group (t = -1.609, d = -0.430, p = 0.111).

The left amygdala activation had no significant main effect of the group (F = 2.870, p = 0.094) and the interaction between the group and run (F = 0.597, p = 0.551). Within the active group, no significant associations were found between changes in MADRS scores and measures of NF training performance, including mean NF amplitude, average left amygdala response during regulation blocks, or changes in left amygdala response from the first to the last training runs (see SI Section 2 for comprehensive details).

Clustering results

In clustering activations related to the regulation block (Fig. 1), the optimal stability score of 0.217 was obtained using the following hyperparameters: averaging responses across runs for each participant, extracting a 40-dimensional UMAP space, and clustering into two subtypes,

which included 32 and 31 participants respectively. In clustering activations related to the feedback event (Fig. 1), the optimal stability score of 0.229 was achieved using a series of responses across three runs, extracting a 14-dimensional UMAP space, and clustering into three subtypes. The subtypes consisted of 23, 15, and 22 participants respectively. No significant association was observed between the subtypes identified in the regulation block and those in the feedback event ($\chi^2 = 3.143$, $p = 0.208$).

Figure 4 shows *t* maps of the mean beta values for the subtypes of regulation block activations (REG subtypes), with detailed peak coordinates provided in SI, Section 3, Table S3. The first subtype, labeled REG-A, exhibited increased BOLD signals within regions commonly identified in neurofeedback (NF) studies, such as the lateral prefrontal cortex, superior and inferior parietal lobules, supplementary motor area (SMA), anterior insula, thalamus, and cerebellum [12]. Conversely, decreased BOLD signals were observed in Heschl's gyrus, posterior insula, middle cingulate cortex, and cuneus. The second subtype, labeled REG-B, showed increased BOLD signals in the lateral prefrontal cortex, SMA, and anterior insula, along with decreased signals in default mode network areas, including the precuneus, posterior cingulate cortex, mediodorsal prefrontal cortex, Rolandic operculum, and fusiform gyrus.

Figure 5 presents *t* maps of the mean beta values for subtypes of the brain responses to the feedback event (FBR subtypes), with peak coordinates detailed in SI, Section 4, Table S4. The first subtype, labeled FBR0, demonstrated a limited response, particularly in the Rolandic operculum and right supramarginal gyrus. The second subtype, labeled FBR-, was characterized by a negative association of BOLD signal changes in response to NF signals over regions including the SMA, middle cingulate cortex, Heschl's gyrus, Rolandic operculum, and visual cortex. In contrast, the third subtype, labeled FBR+, displayed a positive association of BOLD signal changes in areas such as the precuneus, middle cingulate cortex, lateral prefrontal cortex, nucleus accumbens, cerebellum, and inferior occipital regions.

Subtype associations with demographics, NF-training characteristics, and the depressive symptom

Linear model analyses examining associations of the REG and FBR subtypes with age, mean NF signal amplitude, mean left amygdala activation across runs, and baseline MADRS scores revealed no significant differences between the subtypes. Similarly, χ^2 tests showed no significant associations of these subtypes with sex or study participation details (refer to SI section 5 for further detailed statistics).

Changes in MADRS scores were significantly associated with both REG and FBR subtypes, as well as their interaction (REG, $F = 8.735$, $p = 0.005$; FBR, $F = 5.326$, $p = 0.008$; interaction $F = 3.471$, $p = 0.039$). Post-hoc analysis indicated that the REG-B subtype experienced a significant decrease in MADRS scores ($t = -6.077$, $d = -1.702$, $p < 0.001$), in contrast to REG-A ($t = -2.170$, $d = -0.608$, $p = 0.068$). Both FBR- and FBR+ subtypes demonstrated significant decreases in MADRS scores (FBR-: $t = -4.995$, $d = -1.399$, $p < 0.001$; FBR+: $t = -3.818$, $d = -1.069$, $p = 0.001$), whereas the FBR0 subtype did not ($t = -0.839$, $d = -0.235$, $p = 0.786$).

Moreover, changes in MADRS scores varied by subtype combination (Figure 6). A significant reduction was observed when REG-A was paired with FBR- ($t = -3.327$, $d = -0.931$, $p = 0.003$). Within the REG-B group, no significant reduction was seen with FBR0 ($t = -1.221$, $d = -0.342$, $p = 0.401$), but significant reductions occurred when paired with FBR- ($t = -3.789$, $d = -1.061$, $p < 0.001$) and FBR+ ($t = -6.018$, $d = -1.685$, $p < 0.001$). In summary, individuals with MDD classified as REG-A with FBR-, or REG-B with FBR- or FBR+ experienced significant reductions in MADRS scores one week after NF training.

Application of clustering rules to the control group

When the clustering rules of the active group were applied to the control group, 13 and 14 participants were classified into REG-A and REG-B, respectively. For the FBR subtypes, the distribution was 11 participants in FBR0, 5 in FBR-, and 11 in FBR+. No significant association was observed between REG and FBR subtypes within the control group ($\chi^2 = 0.345$, p = 0.842).

Furthermore, the distribution of participants across subtypes did not significantly differ from that in the active group for both REG ($\chi^2 = 0$, $p = 1.000$) and FBR ($\chi^2 = 0.526$, $p = 0.768$) subtypes.

In the control group, subtypes showed no significant associations with age, sex, study participation, mean NF signal amplitude, changes in left amygdala activation, or baseline MADRS scores, as detailed in SI Section 6. Contrary to the active group, the control group exhibited no significant differences in MADRS score changes across subtypes.

Discussion

The primary objective of this study was to identify subtypes of brain activation patterns during NF training that could explain interindividual differences in clinical response. Our analysis revealed significant associations between changes in MADRS scores and subtypes of whole-brain activation patterns during the NF training. However, training characteristics within the target brain region, such as mean NF signal amplitude, mean left amygdala activation, and signal changes in the left amygdala, were not associated with changes in symptoms. In contrast, the control group showed no significant associations between the subtypes and changes in MADRS scores, underscoring that the effects of NF treatment are distinct from placebo effects.

Significant symptom reduction was observed across multiple subtype combinations, indicating the existence of multiple pathways to successful treatment. Notably, individuals classified within the FBR0 subtype, characterized by their non-responsiveness to feedback signals, did not experience significant symptom reduction, highlighting the critical role of feedback response in effective NF training. Significant symptom reduction was evident when individuals responded to feedback signals, whether positively (FBR+) or negatively (FBR-). However, this effect was dependent on their regulation subtype. Individuals exhibiting increased activation across broad brain areas during self-regulation (REG-A), which overlap with areas commonly reported in NF studies [12], required a suppressive response to NF signals (FBR-) to achieve significant symptom

304 reduction. Conversely, individuals who showed increased activation in executive control areas
305 (such as the lateral prefrontal cortex and supplementary motor area) and salience network
306 regions (such as the anterior insula), alongside suppressive activation in the default mode
307 network (DMN) regions during self-regulation (REG-B), achieved symptom reduction regardless
308 of the polarity of their response to feedback signals. These findings suggest that a nonspecific
309 increase in brain activation does not contribute to treatment efficacy; rather, selective
310 modulation of brain responses is crucial for successful NF therapy.

311 Increased activation of the DMN, often linked to self-referential thoughts [53, 54], has been
312 frequently observed in individuals with MDD compared to healthy controls, and is linked to
313 repetitive negative thinking [55-63]. Particularly germane to the pathophysiology of MDD and its
314 treatment mechanisms is the significant role of deactivating the posterior DMN, especially the
315 PCC region. Current evidence suggests that the PCC serves as a major cortical hub for various
316 self-referential phenomena, ranging from spatial body localization to self-talk and
317 autobiographical information processing [64-67]. In this context, the characteristic deactivation of
318 the PCC observed in brain activation subtypes associated with clinical response in our study
319 supports the hypothesis that this region may underlie the persistent and intensified negative
320 self-referential mentation that characterizes depression.

321 Moreover, the absence of suppressive activation during the regulation task can be
322 compensated for by suppressive responses to feedback signals in the supplementary motor
323 area (SMA), middle cingulate, auditory cortex (including Heschl's gyrus and Rolandic
324 operculum), and visual cortex. Although the functional mechanism of these suppressive
325 responses to NF signals remains unclear, they may counteract maladaptive brain activation
326 associated with MDD. In particular, alterations in SMA activity have been reported in MDD [68-71].
327 Changes in SMA and middle cingulate activation were also observed in MDD during reward
328 anticipation in a meta-analysis [72]. In addition, increased connectivity in the auditory cortex,

329 associated with repetitive negative thinking [73], and increased activity or connectivity in the visual
330 cortex [48, 74] have also been reported in MDD.

331 Selective increases and decreases in brain activation associated with successful NF training
332 have also been reported in a meta-analysis of amygdala NF studies [4]. The study found
333 successful amygdala modulation was associated with inactivation in the posterior insula and
334 DMN regions, including the ventromedial prefrontal cortex and posterior cingulate cortex, during
335 the regulation period. Negative activations in the successful modulators were also found in the
336 left parahippocampal gyrus and cuneus, which overlap with the present results of FBR- subtype.
337 Notably, this meta-analysis defined training success as the ability to down-regulate amygdala
338 activation, in contrast to our study, which up-regulated amygdala activation, suggesting a
339 common mechanism in regulating amygdala activity through emotion regulation.

340 In light of the present findings, the therapeutic effects of NF in our study cannot be solely
341 attributed to changes in left amygdala activity. Instead, the process of regulating this activity
342 appears to be crucial for achieving treatment success. This observation aligns with a previous
343 study that has shown activations in brain regions beyond the intended target during NF training
344 can mediate symptom reduction [26]. Such evidence supports the notion that brain self-regulation
345 through NF involves a large-scale network, extending well beyond any single target region.
346 While amygdala activity is a reliable marker of emotional states and has been indicative of
347 successful regulatory efforts in many NF protocols [11], our findings underscore that the amplitude
348 of amygdala regulation alone is not the determinant of therapeutic success. Rather, it is the
349 manner in which this regulation is executed that may account for the observed variability in
350 treatment outcomes.

351 To our knowledge, this study is the first to explore the interindividual differences in brain
352 activation during NF training and its association with therapeutic effects on depressive
353 symptoms. This marks a significant step toward understanding the mechanisms of NF as a
354 treatment for psychiatric disorders. Our findings underscore the importance of the regulation

process over the mere amplitude of amygdala activity, paving the way for advancements in NF protocols. Incorporating feedback that targets both regulation-related activities and responses to feedback could potentially enhance treatment efficacy.

Furthermore, the lack of a significant association between subtypes and pre-existing traits suggests that these subtypes may be modifiable, rather than fixed traits. This opens the possibility of tailoring feedback-based training to foster these modifications. As NF methodologies continue to evolve, focusing on the process of regulating affective states, rather than activating specific brain regions, might yield more effective treatments. In this context, the semantic NF approach, which emphasizes navigating positions within the representational state space over focusing on specific brain activities, offers a promising direction for refining training protocols [75, 76].

The limitations of this study warrant careful consideration. Although the clustering analysis was designed to classify individuals into distinct subtypes, it is possible that these subtypes do not represent distinct groups per se. Rather, the subtypes may be part of a continuous distribution with no clear demarcation between groups. This is suggested by the fact that the obtained optimal stability scores, which indicate the discrepancy between cross-validated solutions, were greater than 0.2, indicating potential ambiguity in cluster definition. In scenarios where the samples have a continuous distribution, splitting into an equal number of participants could emerge as a more stable approach. This phenomenon may explain why our analysis resulted in nearly equal numbers of participants being categorized into each subtype, highlighting that these identified subtypes may not delineate distinct groups but rather capture different facets of the continuous response spectrum.

In conclusion, the present study demonstrates that the therapeutic outcomes of NF training are significantly influenced by whole-brain activation patterns both during the process of affect regulation, and during the response to feedback signals. Our findings reveal multiple patterns of brain activity associated with significant therapeutic effects, suggesting a variety of potential

pathways to recovery through NF training. In future studies, the optimization of NF training may involve real-time monitoring of brain activity during regulation efforts and in response to feedback signals, as well as tailoring feedback signals to the individual's current state of training progress. Such an approach could better tailor the treatment process to each participant's unique neural response patterns, potentially increasing the effectiveness of NF training.

Acknowledgement

This work was supported by the Laureate Institute for Brain Research, NIMH grant K99MH101235, R21MH113871, NIGMS grant P20GM121312, and NARSAD Young Investigator Grant from the Brain and Behavior Research Foundation. The funding sources had no role in the study design, data collection and analysis, decision to publish, or preparation of the manuscript. The authors are solely responsible for the content. The authors would like to acknowledge Jerzy Bodurka, Ph.D. (1964–2021), for his intellectual and scientific contributions to the designing the left amygdala neurofeedback protocols and development of the real-time fMRI neurofeedback systems, which provided the foundation for the present work. During the preparation of this work the authors used ChatGPT (https://chat.openai.com/) and DeepL (https://www.deepl.com/write) in order to improve language and readability. After using these tools, the authors reviewed and edited the content as needed and take full responsibility for the content of the publication.

Conflict of Interest

The authors report no financial relationships with commercial interests in relation to the work described.

References

1. Institute for Health Metrics and Evaluation (IHME). Global Burden of Disease Study 2019. IHME, https://www.healthdata.org/research-analysis/gbd2020.

2. Greenberg PE, Fournier A-A, Sisitsky T, Simes M, Berman R, Koenigsberg SH *et al.* The Economic Burden of Adults with Major Depressive Disorder in the United States (2010 and 2018). *PharmacoEconomics* 2021; **39**(6)**:** 653-665.

3. Pindi P, Houenou J, Piguet C, Favre P. Real-time fMRI neurofeedback as a new treatment for psychiatric disorders: A meta-analysis. *Progress in neuro-psychopharmacology & biological psychiatry* 2022; **119:** 110605.

4. Goldway N, Jalon I, Keynan JN, Hellrung L, Horstmann A, Paret C *et al.* Feasibility and utility of amygdala neurofeedback. *Neurosci Biobehav Rev* 2022; **138:** 104694.

5. Fernandez-Alvarez J, Grassi M, Colombo D, Botella C, Cipresso P, Perna G *et al.* Efficacy of bio- and neurofeedback for depression: a meta-analysis. *Psychological medicine* 2022; **52**(2)**:** 201-216.

6. Trambaiolli LR, Kohl SH, Linden DEJ, Mehler DMA. Neurofeedback training in major depressive disorder: A systematic review of clinical efficacy, study quality and reporting practices. *Neurosci Biobehav Rev* 2021; **125:** 33-56.

7. Taylor SF, Martz ME. Real-time fMRI neurofeedback: the promising potential of brain-training technology to advance clinical neuroscience. *Neuropsychopharmacology : official publication of the American College of Neuropsychopharmacology* 2023; **48**(1)**:** 238-239.

8. Girges C, Vijiaratnam N, Zrinzo L, Ekanayake J, Foltynie T. Volitional Control of Brain Motor Activity and Its Therapeutic Potential. *Neuromodulation* 2022; **25**(8)**:** 1187-1196.

9. Dudek E, Dodell-Feder D. The efficacy of real-time functional magnetic resonance imaging neurofeedback for psychiatric illness: A meta-analysis of brain and behavioral outcomes. *Neurosci Biobehav Rev* 2021; **121:** 291-306.

10. Martz ME, Hart T, Heitzeg MM, Peltier SJ. Neuromodulation of brain activation associated with addiction: A review of real-time fMRI neurofeedback studies. *NeuroImage Clinical* 2020; **27:** 102350.

11. Barreiros AR, Almeida I, Baia BC, Castelo-Branco M. Amygdala Modulation During Emotion Regulation Training With fMRI-Based Neurofeedback. *Frontiers in human neuroscience* 2019; **13:** 89.

12. Emmert K, Kopel R, Sulzer J, Bruhl AB, Berman BD, Linden DEJ *et al.* Meta-analysis of real-time fMRI neurofeedback studies using individual participant data: How is brain regulation mediated? *Neuroimage* 2016; **124**(Pt A)**:** 806-812.

13. Zotev V, Phillips R, Misaki M, Wong CK, Wurfel BE, Krueger F *et al.* Real-time fMRI neurofeedback training of the amygdala activity with simultaneous EEG in veterans with combat-related PTSD. *NeuroImage Clinical* 2018; **19:** 106-121.

14. Herwig U, Lutz J, Scherpiet S, Scheerer H, Kohlberg J, Opialla S *et al.* Training emotion regulation through real-time fMRI neurofeedback of amygdala activity. *Neuroimage* 2019; **184:** 687-696.

15. Paret C, Zahringer J, Ruf M, Gerchen MF, Mall S, Hendler T *et al.* Monitoring and control of amygdala neurofeedback involves distributed information processing in the human brain. *Hum Brain Mapp* 2018; **39**(7)**:** 3018-3031.

16. Lubianiker N, Paret C, Dayan P, Hendler T. Neurofeedback through the lens of reinforcement learning. *Trends Neurosci* 2022; **45**(8)**:** 579-593.

17. Sitaram R, Ros T, Stoeckel L, Haller S, Scharnowski F, Lewis-Peacock J *et al.* Closed-loop brain training: the science of neurofeedback. *Nat Rev Neurosci* 2017; **18**(2)**:** 86-100.

18. Lawrence EJ, Su L, Barker GJ, Medford N, Dalton J, Williams SC *et al.* Self-regulation of the anterior insula: Reinforcement learning using real-time fMRI neurofeedback. *Neuroimage* 2014; **88:** 113-124.

19. Skottnik L, Sorger B, Kamp T, Linden D, Goebel R. Success and failure of controlling the real-time functional magnetic resonance imaging neurofeedback signal are reflected in the striatum. *Brain Behav* 2019; **9**(3)**:** e01240.

20. Sutton RS, Barto AG. *Reinforcement learning: An introduction*. 2nd edn. MIT Press Cambridge, MA2018.

21. Young KD, Zotev V, Phillips R, Misaki M, Yuan H, Drevets WC *et al.* Real-time FMRI neurofeedback training of amygdala activity in patients with major depressive disorder. *PLoS One* 2014; **9**(2)**:** e88785.

22. Young KD, Siegle GJ, Bodurka J, Drevets WC. Amygdala Activity During Autobiographical Memory Recall in Depressed and Vulnerable Individuals: Association With Symptom Severity and Autobiographical Overgenerality. *Am J Psychiatry* 2016; **173**(1)**:** 78-89.

23. Yuan H, Young KD, Phillips R, Zotev V, Misaki M, Bodurka J. Resting-state functional connectivity modulation and sustained changes after real-time functional magnetic resonance imaging neurofeedback training in depression. *Brain connectivity* 2014; **4**(9)**:** 690-701.

24. Tsuchiyagaito A, Smith JL, El-Sabbagh N, Zotev V, Misaki M, Al Zoubi O *et al.* Real-time fMRI neurofeedback amygdala training may influence kynurenine pathway metabolism in major depressive disorder. *NeuroImage Clinical* 2021; **29:** 102559.

25. Misaki M, Mulyana B, Zotev V, Wurfel BE, Krueger F, Feldner M *et al.* Hippocampal volume recovery with real-time functional MRI amygdala neurofeedback emotional

training for posttraumatic stress disorder. *Journal of affective disorders* 2021; **283:** 229-235.

26. Misaki M, Phillips R, Zotev V, Wong CK, Wurfel BE, Krueger F *et al.* Brain activity mediators of PTSD symptom reduction during real-time fMRI amygdala neurofeedback emotional training. *NeuroImage Clinical* 2019; **24:** 102047.

27. Misaki M, Phillips R, Zotev V, Wong CK, Wurfel BE, Krueger F *et al.* Real-time fMRI amygdala neurofeedback positive emotional training normalized resting-state functional connectivity in combat veterans with and without PTSD: a connectome-wide investigation. *NeuroImage Clinical* 2018; **20:** 543-555.

28. American Psychiatric Association. *Diagnostic and Statistical Manual of Mental Disorders DSM-IV-TR Fourth Edition (Text Revision)*. American Psychiatric Publishing: Washington, DC, 2000.

29. First MB. Structured clinical interview for DSM‐IV‐TR axis I disorders, research version, patient edition (SCID‐I/P). *Biometrics research*: New York, NY, 2002.

30. Sheehan DV, Lecrubier Y, Sheehan KH, Amorim P, Janavs J, Weiller E *et al.* The Mini-International Neuropsychiatric Interview (M.I.N.I.): the development and validation of a structured diagnostic psychiatric interview for DSM-IV and ICD-10. *The Journal of clinical psychiatry* 1998; **59 Suppl 20:** 22-33;quiz 34-57.

31. Zotev V, Krueger F, Phillips R, Alvarez RP, Simmons WK, Bellgowan P *et al.* Self-regulation of amygdala activation using real-time FMRI neurofeedback. *PLoS One* 2011; **6**(9)**:** e24522.

32. Montgomery SA, Åsberg M. A new depression scale designed to be sensitive to change. *The British journal of psychiatry : the journal of mental science* 1979; **134:** 382-389.

33. Fias W, Lammertyn J, Caessens B, Orban GA. Processing of Abstract Ordinal Knowledge in the Horizontal Segment of the Intraparietal Sulcus. *The Journal of Neuroscience* 2007; **27**(33)**:** 8952-8956.

34. Glover GH, Li TQ, Ress D. Image-based method for retrospective correction of physiological motion effects in fMRI: RETROICOR. *Magn Reson Med* 2000; **44**(1)**:** 162-167.

35. Birn RM, Smith MA, Jones TB, Bandettini PA. The respiration response function: the temporal dynamics of fMRI signal fluctuations related to changes in respiration. *Neuroimage* 2008; **40**(2)**:** 644-654.

36. Jo HJ, Saad ZS, Simmons WK, Milbury LA, Cox RW. Mapping sources of correlation in resting state FMRI, with artifact detection and removal. *Neuroimage* 2010; **52**(2)**:** 571-582.

37. Mumford JA, Turner BO, Ashby FG, Poldrack RA. Deconvolving BOLD activation in event-related designs for multivoxel pattern classification analyses. *Neuroimage* 2012; **59**(3)**:** 2636-2643.

38. Chen G, Taylor PA, Stoddard J, Cox RW, Bandettini PA, Pessoa L. Sources of Information Waste in Neuroimaging: Mishandling Structures, Thinking Dichotomously, and Over-Reducing Data. *Aperture Neuro* 2022; **2:** 1-22.

39. Chen G, Padmala S, Chen Y, Taylor PA, Cox RW, Pessoa L. To pool or not to pool: Can we ignore cross-trial variability in FMRI? *Neuroimage* 2021; **225:** 117496.

40. Altman N, Krzywinski M. The curse(s) of dimensionality. *Nature methods* 2018; **15**(6)**:** 399-400.

41. McInnes L, Healy J, Melville J. Umap: Uniform manifold approximation and projection for dimension reduction. *arXiv preprint arXiv:180203426* 2018.

42. Landi I, Mandelli V, Lombardo MV. reval: A Python package to determine best clustering solutions with stability-based relative clustering validation. *Patterns (N Y)* 2021; **2**(4)**:** 100228.

43. Shen X, Finn ES, Scheinost D, Rosenberg MD, Chun MM, Papademetris X *et al.* Using connectome-based predictive modeling to predict individual behavior from brain connectivity. *Nature protocols* 2017; **12**(3)**:** 506-518.

44. Shen X, Tokoglu F, Papademetris X, Constable RT. Groupwise whole-brain parcellation from resting-state fMRI data for network node identification. *Neuroimage* 2013; **82:** 403-415.

45. Greene AS, Gao S, Scheinost D, Constable RT. Task-induced brain state manipulation improves prediction of individual traits. *Nature communications* 2018; **9**(1)**:** 2807.

46. Greene AS, Gao S, Noble S, Scheinost D, Constable RT. How Tasks Change Whole-Brain Functional Organization to Reveal Brain-Phenotype Relationships. *Cell Rep* 2020; **32**(8)**:** 108066.

47. Ju S, Horien C, Shen X, Abuwarda H, Trainer A, Constable RT *et al.* Connectome-based predictive modeling shows sex differences in brain-based predictors of memory performance. *Frontiers in Dementia* 2023; **2**.

48. Misaki M, Tsuchiyagaito A, Guinjoan SM, Rohan ML, Paulus MP. Trait repetitive negative thinking in depression is associated with functional connectivity in negative thinking state rather than resting state. *Journal of affective disorders* 2023; **340:** 843-854.

49. Yoo K, Rosenberg MD, Hsu WT, Zhang S, Li CR, Scheinost D *et al.* Connectome-based predictive modeling of attention: Comparing different functional connectivity features and prediction methods across datasets. *Neuroimage* 2018; **167:** 11-22.

50. Lange T, Roth V, Braun ML, Buhmann JM. Stability-Based Validation of Clustering Solutions. *Neural Computation* 2004; **16**(6)**:** 1299-1323.

51. Bates D, Mächler M, Bolker B, Walker S. Fitting Linear Mixed-Effects Models Usinglme4. *Journal of Statistical Software* 2015; **67**(1)**:** 1–48.

52. emmeans: Estimated Marginal Means, aka Least-Squares Means. https://CRAN.R-project.org/package=emmeans, 2022, Accessed Date Accessed 2022 Accessed.

53. Axelrod V, Rees G, Bar M. The default network and the combination of cognitive processes that mediate self-generated thought. *Nature Human Behaviour* 2017; **1**(12)**:** 896-910.

54. Andrews-Hanna JR, Smallwood J, Spreng RN. The default network and self-generated thought: component processes, dynamic control, and clinical relevance. *Annals of the New York Academy of Sciences* 2014; **1316**(1)**:** 29-52.

55. Hamilton JP, Farmer M, Fogelman P, Gotlib IH. Depressive Rumination, the Default-Mode Network, and the Dark Matter of Clinical Neuroscience. *Biol Psychiatry* 2015; **78**(4)**:** 224-230.

56. Wise T, Marwood L, Perkins AM, Herane-Vives A, Joules R, Lythgoe DJ *et al.* Instability of default mode network connectivity in major depression: a two-sample confirmation study. *Translational psychiatry* 2017; **7**(4)**:** e1105.

57. Zhu X, Zhu Q, Shen H, Liao W, Yuan F. Rumination and Default Mode Network Subsystems Connectivity in First-episode, Drug-Naive Young Patients with Major Depressive Disorder. *Sci Rep* 2017; **7:** 43105.

58. Bessette KL, Jenkins LM, Skerrett KA, Gowins JR, DelDonno SR, Zubieta JK *et al.* Reliability, Convergent Validity and Time Invariance of Default Mode Network Deviations in Early Adult Major Depressive Disorder. *Front Psychiatry* 2018; **9:** 244.

59. Jacob Y, Morris LS, Huang KH, Schneider M, Rutter S, Verma G *et al.* Neural correlates of rumination in major depressive disorder: A brain network analysis. *NeuroImage Clinical* 2020; **25:** 102142.

60. Makovac E, Fagioli S, Rae CL, Critchley HD, Ottaviani C. Can't get it off my brain: Meta-analysis of neuroimaging studies on perseverative cognition. *Psychiatry Res Neuroimaging* 2020; **295:** 111020.

61. Misaki M, Tsuchiyagaito A, Al Zoubi O, Paulus M, Bodurka J, Tulsa I. Connectome-wide search for functional connectivity locus associated with pathological rumination as a target for real-time fMRI neurofeedback intervention. *NeuroImage Clinical* 2020; **26:** 102244.

62. Stern ER, Eng GK, De Nadai AS, Iosifescu DV, Tobe RH, Collins KA. Imbalance between default mode and sensorimotor connectivity is associated with perseverative thinking in obsessive-compulsive disorder. *Translational psychiatry* 2022; **12**(1)**:** 19.

63. Yang MH, Guo ZP, Lv XY, Zhang ZQ, Wang WD, Wang J *et al.* BMRMI Reduces Depressive Rumination Possibly through Improving Abnormal FC of Dorsal ACC. *Neural Plast* 2022; **2022:** 8068988.

64. Agathos J, Steward T, Davey CG, Felmingham KL, Ince S, Moffat BA *et al.* Differential engagement of the posterior cingulate cortex during cognitive restructuring of negative self- and social beliefs. *Social cognitive and affective neuroscience* 2023; **18**(1).

65. Natu VS, Lin JJ, Burks A, Arora A, Rugg MD, Lega B. Stimulation of the Posterior Cingulate Cortex Impairs Episodic Memory Encoding. *J Neurosci* 2019; **39**(36)**:** 7173-7182.

66. Guterstam A, Bjornsdotter M, Gentile G, Ehrsson HH. Posterior cingulate cortex integrates the senses of self-location and body ownership. *Curr Biol* 2015; **25**(11)**:** 1416-1425.

67. Foster BL, Koslov SR, Aponik-Gremillion L, Monko ME, Hayden BY, Heilbronner SR. A tripartite view of the posterior cingulate cortex. *Nat Rev Neurosci* 2023; **24**(3)**:** 173-189.

68. Andreescu C, Butters M, Lenze EJ, Venkatraman VK, Nable M, Reynolds III CF *et al.* fMRI activation in late-life anxious depression: a potential biomarker. *International Journal of Geriatric Psychiatry* 2009; **24**(8)**:** 820-828.

69. Ionescu DF, Niciu MJ, Mathews DC, Richards EM, Zarate Jr CA. NEUROBIOLOGY OF ANXIOUS DEPRESSION: A REVIEW. *Depression and Anxiety* 2013; **30**(4)**:** 374-385.

70. Sarkheil P, Odysseos P, Bee I, Zvyagintsev M, Neuner I, Mathiak K. Functional connectivity of supplementary motor area during finger-tapping in major depression. *Comprehensive psychiatry* 2020; **99:** 152166.

71. Northoff G, Hirjak D, Wolf RC, Magioncalda P, Martino M. All roads lead to the motor cortex: psychomotor mechanisms and their biochemical modulation in psychiatric disorders. *Molecular psychiatry* 2021; **26**(1)**:** 92-102.

72. Jauhar S, Fortea L, Solanes A, Albajes-Eizagirre A, McKenna PJ, Radua J. Brain activations associated with anticipation and delivery of monetary reward: A systematic review and meta-analysis of fMRI studies. *PLOS ONE* 2021; **16**(8)**:** e0255292.

73. Tsuchiyagaito A, Sanchez SM, Misaki M, Kuplicki R, Park H, Paulus MP *et al.* Intensity of repetitive negative thinking in depression is associated with greater functional connectivity between semantic processing and emotion regulation areas. *Psychological medicine* 2023; **53**(12)**:** 5488-5499.

74. Wu F, Lu Q, Kong Y, Zhang Z. A Comprehensive Overview of the Role of Visual Cortex Malfunction in Depressive Disorders: Opportunities and Challenges. *Neuroscience Bulletin* 2023; **39**(9)**:** 1426-1438.

75. Ciarlo A, Russo AG, Ponticorvo S, di Salle F, Lührs M, Goebel R *et al.* Semantic fMRI neurofeedback: a multi-subject study at 3 tesla. *Journal of Neural Engineering* 2022; **19**(3)**:** 036020.

76. Russo AG, Luhrs M, Di Salle F, Esposito F, Goebel R. Towards semantic fMRI neurofeedback: navigating among mental states using real-time representational similarity analysis. *J Neural Eng* 2021; **18**(4)**:** 046015.

Figure legends

Figure 1. Schematic diagram of the neurofeedback-based brain regulation training loop (left panel) and the models used to estimate brain activation at each epoch (right panel). The reinforcement learning process is typically characterized by the evaluation of a feedback signal followed by the adjustment of action (mental regulation) to increase the reward (feedback) signal. Brain activations corresponding to these two components were analyzed using an event-related response model for each neurofeedback presentation at every TR, modulated by feedback amplitude, and a block-wise response model during the neurofeedback regulation blocks.

Figure 2. Procedures of clustering whole-brain beta maps

Figure 3: MADRS scores before and after NF training in the active and control groups. The bars show the mean MADRS scores for each group, with the error bars representing their standard error. Individual participant scores are shown as dots, with lines connecting pre- and post-training scores to highlight changes for each individual. A statistically significant decrease in post-training MADRS scores was observed in the active group (***, $p < 0.001$).

Figure 4. *t* maps of mean activation in the regulation block for the REG subtypes. The maps are thresholded at a voxel-wise $p < 0.001$, with cluster-size correction at $p < 0.05$.

Figure 5. *t* maps of mean activation in response to NF signals for the FBR subtypes. The maps are thresholded at a voxel-wise $p < 0.001$, with cluster-size correction at $p < 0.05$.

Figure 6. Ratio of change in MADRS score from baseline for each REG and FBR subtype. **, $p < 0.005$; ***, $p < 0.001$.

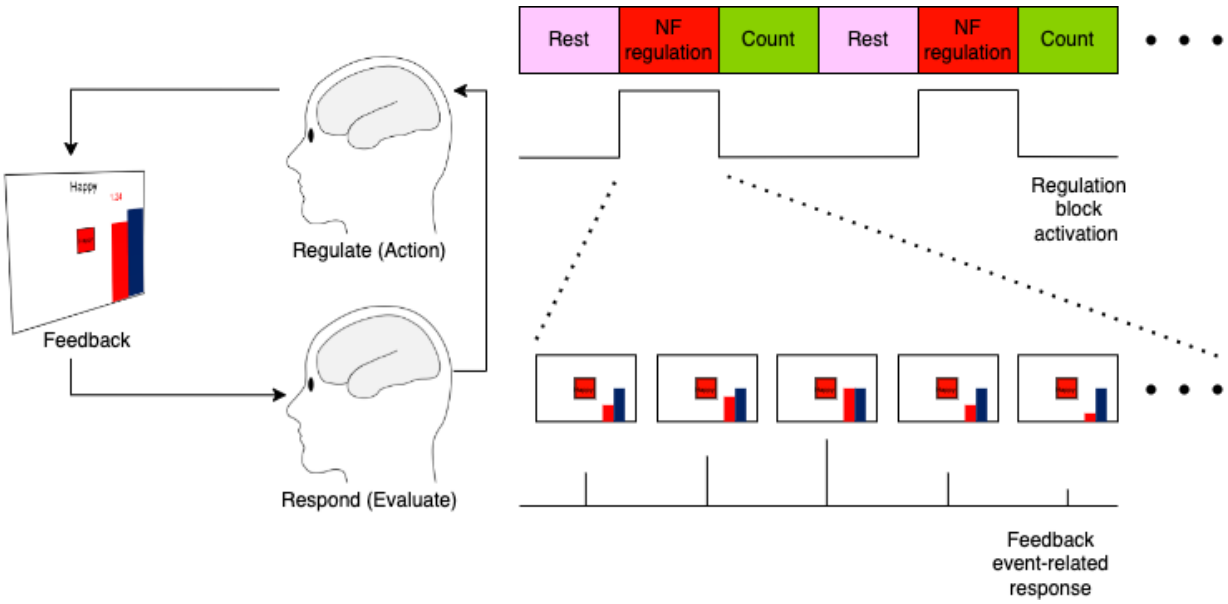
Rest
NF regulation
Count
Rest
NF regulation
Count
Regulate (Action)
Feedback
Respond (Evaluate)
Regulation block activation
Feedback event-related response

Figure 1

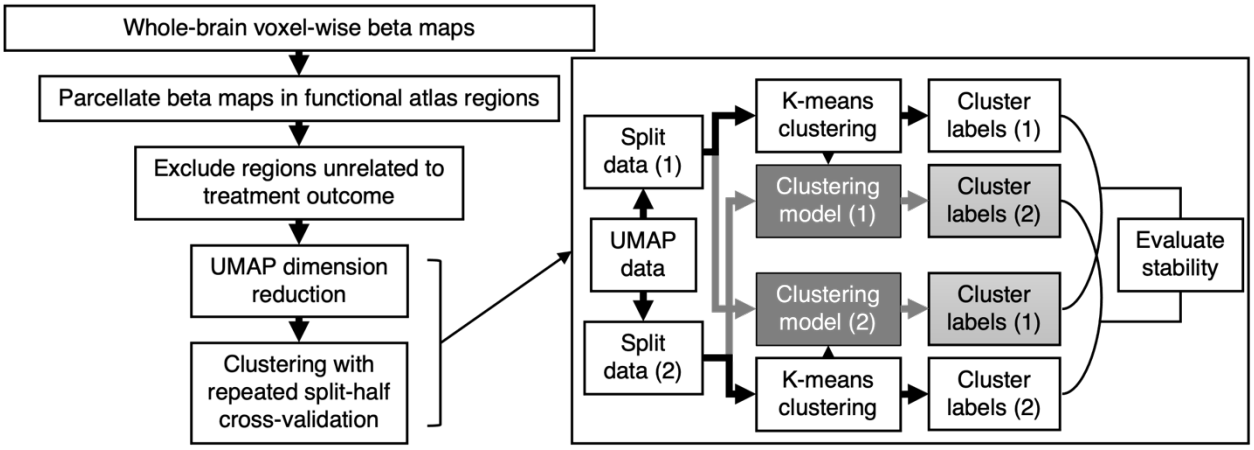
Whole-brain voxel-wise beta maps
Parcellate beta maps in functional atlas regions
Exclude regions unrelated to treatment outcome
UMAP dimension reduction
Clustering with repeated split-half cross-validation
Split data (1)
UMAP data
Split data (2)
K-means clustering
Clustering model (1)
Clustering model (2)
K-means clustering
Cluster labels (1)
Cluster labels (2)
Cluster labels (1)
Cluster labels (2)
Evaluate stability

Figure 2

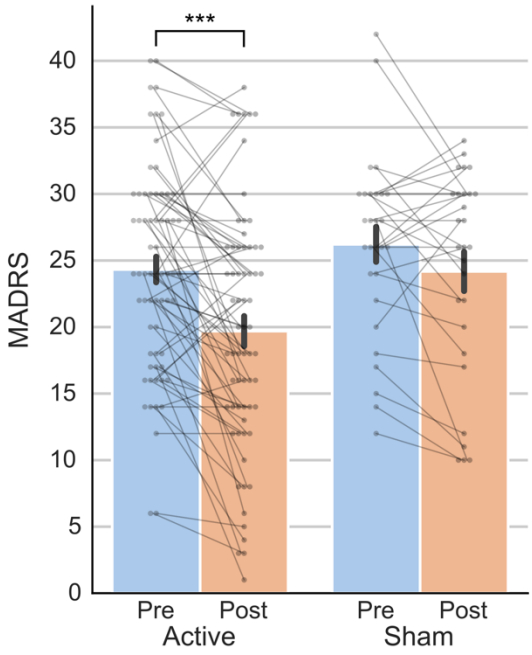

Figure 3

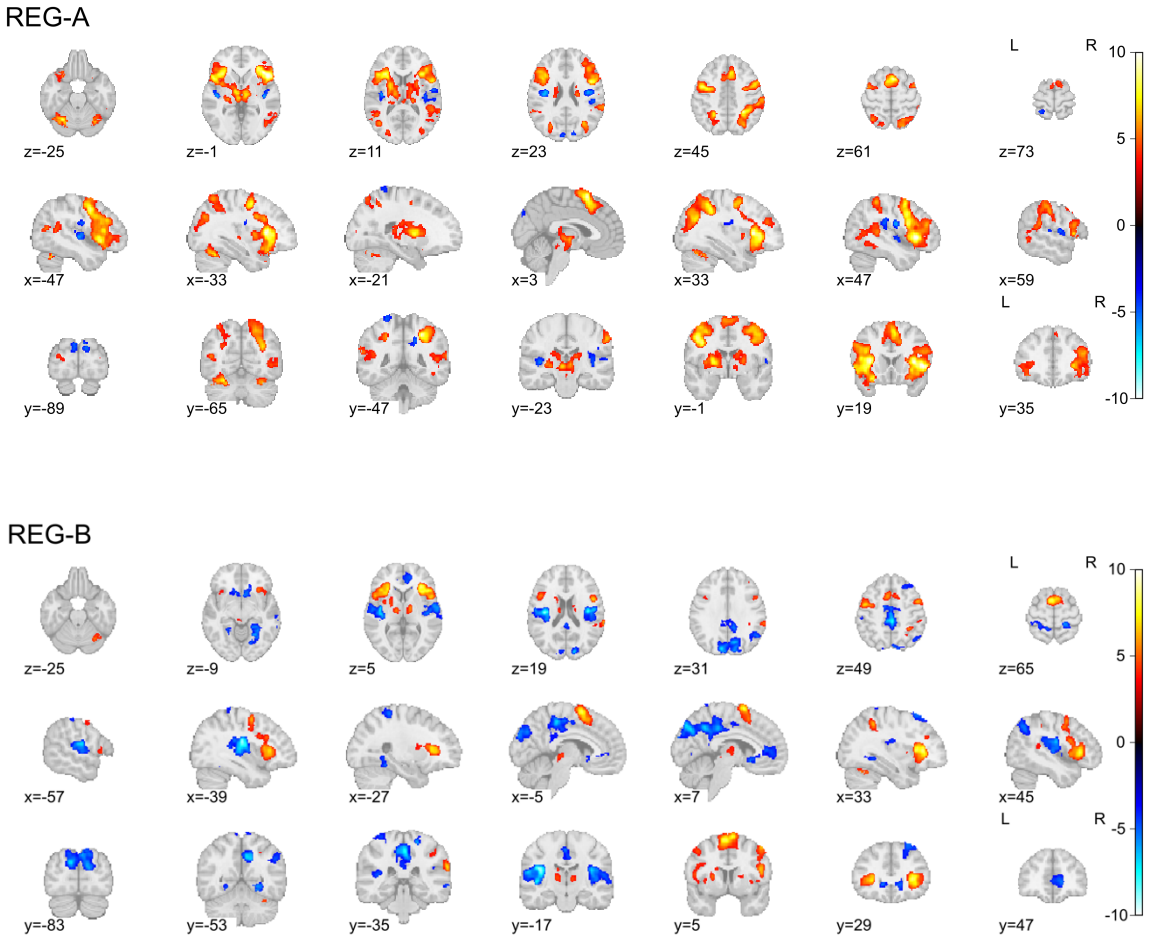
REG-A
z=-25
z=-1
z=11
z=23
z=45
z=61
z=73
x=-47
x=-33
x=-21
x=3
x=33
x=47
x=59
y=-89
y=-65
y=-47
y=-23
y=-1
y=19
y=35
L
R
10
5
0
-5
-10
REG-B
z=-25
z=-9
z=5
z=19
z=31
z=49
z=65
x=-57
x=-39
x=-27
x=-5
x=7
x=33
x=45
y=-83
y=-53
y=-35
y=-17
y=5
y=29
y=47

Figure 4

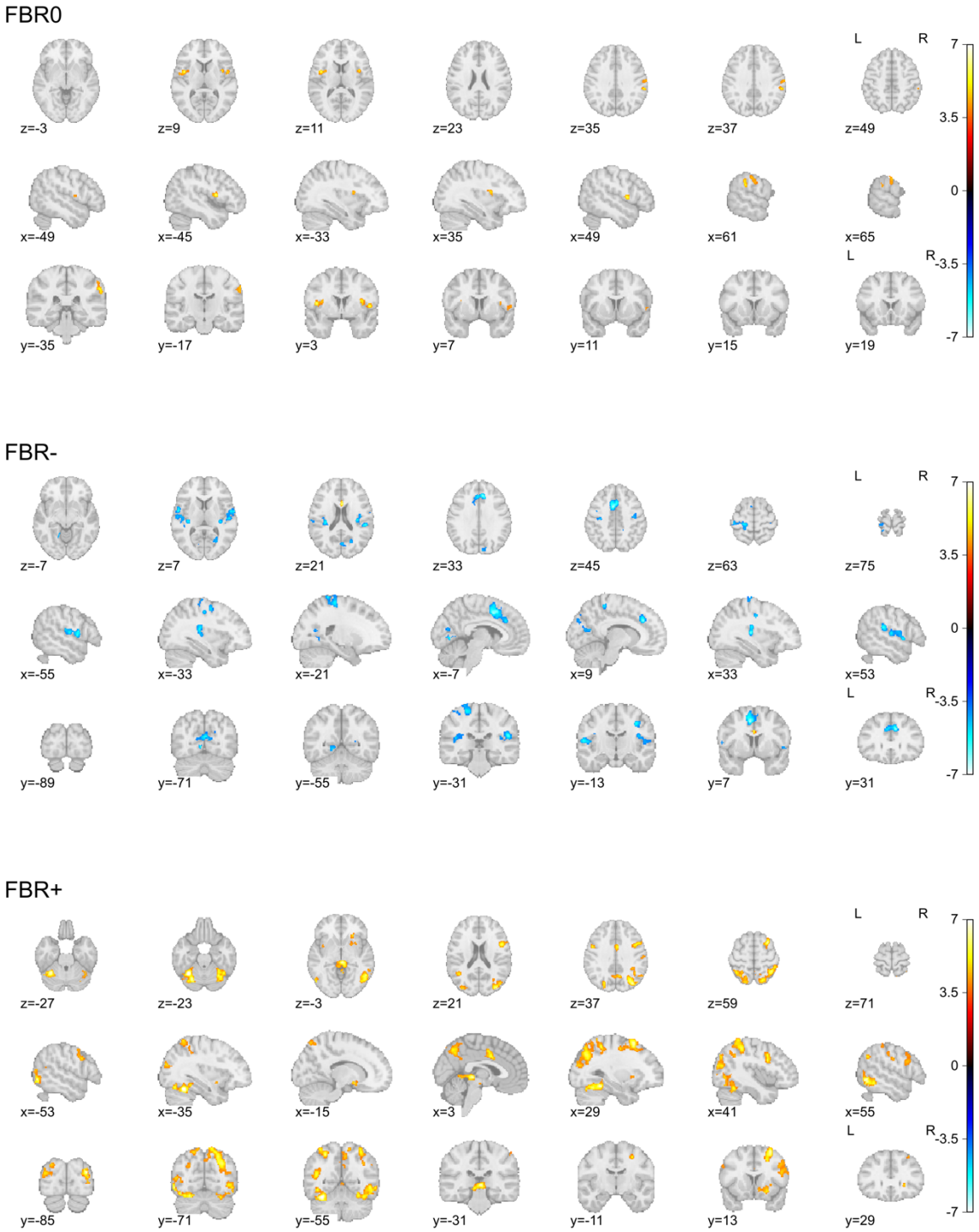
FBR0
z=-3
z=9
z=11
z=23
z=35
z=37
z=49
x=-49
x=-45
x=-33
x=35
x=49
x=61
x=65
y=-35
y=-17
y=3
y=7
y=11
y=15
y=19
L
R
7
3.5
0
-3.5
-7
FBR-
z=-7
z=7
z=21
z=33
z=45
z=63
z=75
x=-55
x=-33
x=-21
x=-7
x=9
x=33
x=53
y=-89
y=-71
y=-55
y=-31
y=-13
y=7
y=31
FBR+
z=-27
z=-23
z=-3
z=21
z=37
z=59
z=71
x=-53
x=-35
x=-15
x=3
x=29
x=41
x=55
y=-85
y=-71
y=-55
y=-31
y=-11
y=13
y=29

Figure 5

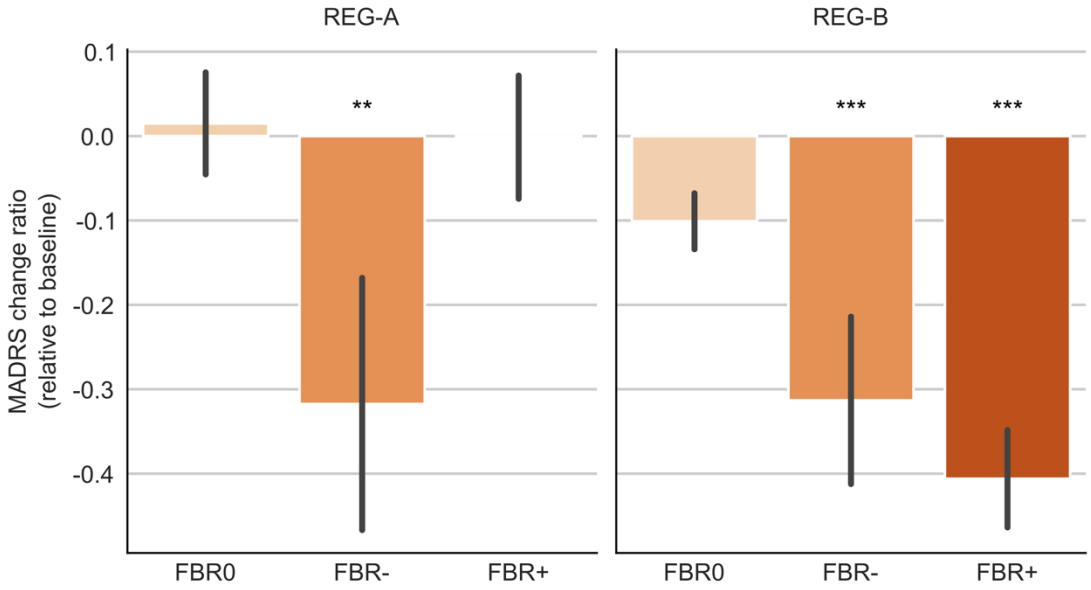
REG-A
REG-B
MADRS change ratio
(relative to baseline)
0.1
0.0
-0.1
-0.2
-0.3
-0.4
**
***
***
FBR0
FBR-
FBR+
FBR0
FBR-
FBR+

Figure 6